


RESEARCH ARTICLE OPEN ACCESS

Subterranean Mine Inspection Using the Prometheus Re-Configurable Drone

Liam Brown¹ | Robert Clarke² | Ali Akbari³ | Ferdian Jovan⁴ | Jameel Marafie⁵ | Ognjen Marjanovic¹ | Sara Bernardini⁶ | Tom Richardson² | Simon Watson¹ 

¹Department of Electrical and Electronic Engineering, The University of Manchester, Manchester, UK | ²Faculty of Science and Engineering, University of Bristol, Bristol, UK | ³Department of Computer Science, Royal Holloway University of London, Egham, UK | ⁴School of Natural and Computing Sciences, University of Aberdeen, Aberdeen, UK | ⁵Headlight AI, Brighton, UK | ⁶Department of Computer Science, University of Oxford, Oxford, UK

Correspondence: Simon Watson (simon.watson@manchester.ac.uk)

Received: 29 October 2024 | **Revised:** 3 June 2025 | **Accepted:** 25 October 2025

Funding: This study has been completed in partnership with the following companies that have provided insight and technical expertise to the project: Callen-Lenz, Headlight AI Limited, Network Rail Infrastructure Limited and Thales UK Limited. Prometheus (104824) was funded through the Industrial Strategy Challenge Fund under the Robotics and AI in Extreme Environments challenge. The Industrial Strategy Challenge Fund is delivered by UK Research and Innovation. It was also funded by the Robotics and AI Hub (RAIN Hub) EP/R026084/1.

ABSTRACT

This paper describes the design, development, and real-world testing of an autonomous drone for subterranean exploration, known as “Prometheus.” Driven by requirements from industry that the drone be able to be deployed through areas of restricted access, Prometheus was designed to be directly deployed through a 150 mm aperture. This diameter was chosen because of its propensity in industry, such as access into caves and other confined environments. It can subsequently unfold and automatically undock itself from its deployment system, before achieving full flight capabilities. This paper presents results obtained during a deployment at Holman’s test mine in Cornwall, UK. The mine is an old granite quarry that has over 2 km of tunnels and is a representative environment in which the Prometheus drone was shown to be an ideal system with which to explore and map unknown voids with restricted borehole access.

1 | Introduction

The exploration and inspection of subterranean environments have been the focus of significant research over the last 5 years, culminating in the DARPA Subterranean challenge (SubT), which ran its final event in September 2021 (Tranzatto et al. 2022). The aim of the DARPA SubT challenge was to demonstrate the ability of teams of ground and aerial robots to explore large unknown subterranean environments autonomously (Rouček et al. 2020). Within the DARPA SubT challenge, there were three courses: cave, tunnel, urban (Petrlik et al. 2025). The entrances to these courses, where the robots could be deployed, were

approximately 2.5 m wide by 2.2 m tall, as shown in Figure 1a (DARPA 2020). This essentially meant that there were no constraints on the types of ground or aerial robots that could be deployed.

There are, however, many subterranean environments where access is much more restricted. Examples include entrances into mines, where access is typically heavily restricted by natural phenomena, or the entrance into an industrial facility, where, to protect workers, access may be constrained to be through 150 mm access ways. This is particularly the case in the nuclear industry, where there are many examples of access ways being restricted (Cheah et al. 2023). In these scenarios,

Liam Brown, Robert Clarke, Ali Akbari and Ferdian Jovan are contributed equally to this work.

This is an open access article under the terms of the [Creative Commons Attribution](https://creativecommons.org/licenses/by/4.0/) License, which permits use, distribution and reproduction in any medium, provided the original work is properly cited.

© 2025 The Author(s). *Journal of Field Robotics* published by Wiley Periodicals LLC.

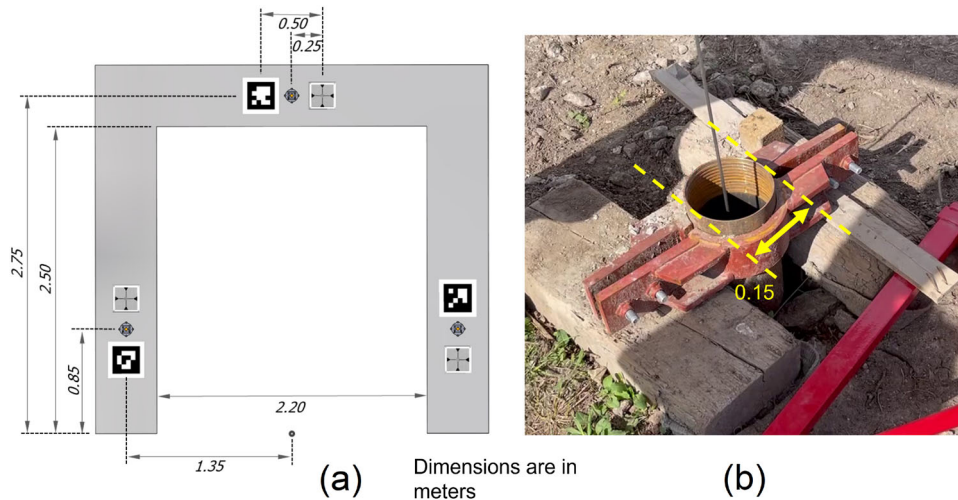


FIGURE 1 | (a) 2.5 m entry portal for DARPA SubT Cave Challenge (DARPA 2020), (b) the 150 mm borehole for remote mine inspection tested with the Prometheus drone. [Color figure can be viewed at [wileyonlinelibrary.com](https://onlinelibrary.wiley.com/doi/10.1002/rob.7012)]

limited sensor data can be gathered by deploying fixed sensors down small bore holes (Vadillo et al. 2012). Figure 1b shows an example 150 mm bore hole drilled into the Holman's Test mine in Cornwall, UK. The test mine also allowed human entry into the mine during the deployment so that flight operations could be observed.

When the entry port into a mine or cave is restricted to 150 mm, traditional robots, such as those used in the DARPA SubT challenge or other similar projects (Azpúrua et al. 2021; Petris et al. 2022), cannot be deployed. A specific use case with this deployment restriction is the inspection of subterranean mines that are below critical rail infrastructure. These need to be monitored regularly to monitor and ensure their stability and to identify if any preventative measures need to be taken to guarantee it (Rail 2019). A 150 mm diameter bore hole is relatively easy to drill, whereas providing physical access for inspectors is far more difficult and expensive to provide. The subterranean voids themselves can be complex and extensive three-dimensional forms which can only be fully explored using robotic technologies. Because of this, a fully autonomous, re-configurable drone that is capable of ingress and egress via 150 mm bore hole access is highly desirable.

1.1 | Design Requirements

There are a number of challenging constraints that need to be addressed within the design of a drone for borehole deployment into restricted access environments. Whilst the design requirements listed in this paper were derived for the subterranean mine scenario, they are generalizable to many other constrained access environments.

- The drone must be deployable through a 150 mm diameter borehole
- The length of the borehole from the surface to the ceiling of the mine cavern may be up to 30 m
- The drone must autonomously detach from the deployment mechanism

- The drone must be able to undertake an autonomous exploration or navigation mission, with no human interaction, in a mine which will be GPS denied and with little or no ambient light available
- The drone must be able to carry an environmental sensor payload for three-dimensional mapping
- Once a mission is complete, the drone must return to the surface with minimal human intervention

To address these challenging design requirements, the Prometheus project was established. Previous published work on this project (Brown et al. 2020) presented the initial design of a re-configurable drone which could be deployed through the 150 mm borehole. This paper presents the complete Prometheus system, including deployment and docking systems, autonomous flight mode and the results of a real-world deployment into Holman's test mine in Cornwall, UK, in July 2021.

2 | Related Work

A comprehensive survey on the autonomous exploration of confined subterranean environments is presented in Azpúrua et al. (2023), which covers in detail the current state-of-the-art in sensors and autonomous exploration, including results from the DARPA SubT Challenge. One area which is not covered in detail is the hardware platforms, acting as sensor deployment tools, which will be the focus of this review.

2.1 | Reconfigurable, Transformable, Folding, or Changing Morphology Drones

The majority of drones used for the exploration of subterranean or indoor confined spaces make use of fixed configuration multi-rotors (Tranzatto et al. 2022; Krátký et al. 2021; Hudson et al. 2022; Agha et al. 2022; Lindqvist et al. 2022). These can range in size from small (212 mm tip-to-tip, 0.3 kg) drones with

limited payloads (small visual cameras) (Tavasoli et al. 2023) up to large drones (1250 mm tip-to-tip, 6 kg) which can carry a full navigational and environmental sensor payload (Schleich et al. 2021). None of these drones, however, is physically capable of being deployed through 150 mm diameter boreholes. Drones with a diameter of less than 150 mm can be purchased commercially; however, they trade size for functionality as they only have a low-quality camera for sensing.

Drones which can change their configuration either during or before flight have become a topic of research interest over the last few years. Terms to describe these drones include reconfigurable, transformable, folding, or changing morphology. One of the earliest morphing drones was presented by Zhou et al. in 2017 (Zhao et al. 2017). They offered a transformable aerial robot platform made up of four links. Each link was 400 mm in length with a diameter of 310 mm and a total drone mass of 2.05 kg. During flight, the drone could change its shape from a classic quadrotor configuration into a curved configuration and was used to grasp objects of interest. This system then evolved into the DRAGON drone (Dual-rotor embedded multilink Robot with the Ability of multi-deGree-of-freedom aerial transformation) (Zhao et al. 2018), which was designed to pass through narrow openings. Each link had a diameter of 424 mm, and the total mass of the drone was 7.38 kg. Neither of these drones had a sensor payload beyond onboard IMUs and used motion capture systems for localization.

Riviere et al. (2018) developed a folding drone in 2018, which utilized a different approach to the DRAGON drone. Their Quad-Morphing drone had two arms, at the end of which was a rotating arm with two propellers on it. When the end arms were orthogonal to the fixed arms, the drone had a classic X morphology. However, the end arms could be rotated by 90° so that all of the propellers were in a line down the fixed arms. In the unfolded configuration, the drone had a maximum width of 268 mm, whilst in the folded configuration, this was reduced to 128 mm. The drone had a payload of 0.4 kg, but it was not flown outside of a lab environment, and there was no mechanism which would enable it to be deployed in the folded configuration.

A drone with actuated elbow joints was developed by Devlin et al. in 2018 (Devlin et al. 2018). The ElbowQuad drone was based on a standard quadrotor platform, but each of the rotor arms included an actuated joint which allowed the drone to reduce its footprint. No dimensions were provided in the publication for the size of the drone beyond stating that the motors used were appropriate for 250–300 mm quadrotors.

In 2019, Falanga et al. presented a foldable drone which could change its shape during flight (Falanga et al. 2019). Unlike the DRAGON drone, this platform was based around a traditional quadrotor morphology; a fixed central rigid body but with four foldable rotor arms. The drone had four different configurations: the conventional X shape, an H shape, an O shape, and a T shape. In the X morphology, the tip-to-tip diameter was 470 mm, and the drone had a mass of 0.58 kg. The most compact morphology was the O configuration, which reduced the overall tip-to-tip diameter to 391 mm.

Bucki et al. developed a passively morphing quadcopter in 2019 (Bucki and Mueller 2019) which used springs and the rotor thrust forces to reconfigure into different shapes. The tip-to-tip diameter of the drone in the default X configuration was 540 mm, and, in the folded configuration, this was reduced to 280 mm. The mass of the drone was 940 g. The drone was successfully flown in a lab environment in its reconfigured form.

Another class of reconfigurable drones, which has seen development in recent years, are ballistically launched drones. These drones start in a compact form with their rotor arms passively folded using spring-based systems. When launched, the arms expand into a classic X configuration for flight. Systems such as SQUID (Streamlined Quick Unfolding Investigation Drone) (Bouman et al. 2020) (150 mm compact form and 580 mm unfolded diameter) and the commercially available Ninox 40 MT (Paolo Valpolini 2020) (40 mm diameter in the compact form) have demonstrated the feasibility of such systems; however, they are not able to reconfigure back into their compact form.

There are several other commercial reconfigurable drones which have been released, including the PowerVision PowerEgg (PowerVision 2023), which can reconfigure from a compact tip-to-tip diameter of 176 mm up to a flight diameter 476 mm; the LevelTop Smart Drone, which has a compact diameter of 86 mm and a flight diameter of 237 mm (LevelTop T1 2018); and the Ascent Aerosystems Spirit Coaxial drone (Aerosystems 2023), which in compact form has a diameter of 106 mm and a flight tip-to-tip diameter of 648 mm.

Table 1 shows the different reconfigurable drones analyzed against the design requirements from Section 1.1. The last entry is the Prometheus Titan drone, which was designed during this project. As you can see, there are no existing drones, except the Prometheus Titan, which meets the unique requirements of deployment and retrieval through a 150 mm borehole and autonomous navigation in a dark, GPS-denied environment.

2.2 | Drone Docking Systems

The Prometheus project requires the drone to be deployed down a borehole, launched, then retrieved and pulled back to the surface. This necessitates a docking mechanism which can both launch and recover the drone from the ceiling entry point where the borehole exits into the mine. The majority of existing docking systems assume that the drone is being launched from, or is landing on, a planar surface below it, Galimov et al. (2020); Grlj et al. (2022). This may be a fixed dock or landing platform, or another robot, such as an autonomous ground robot (Cheng et al. 2022; Deng et al. 2023).

Vertical docking systems are not very common in the literature, as the use cases for their adoption are relatively limited. Lieret et al. proposed an overhead docking and charging station in 2021 (Lieret et al. 2021). The drone used UWB tracking for localization to position itself beneath the dock. It then used an upward-facing camera and fiducial markers on the dock for precision alignment. The drone had a conical centring device

TABLE 1 | Comparison of reconfigurable drones.

Drone	Year	≤ 150 mm Compact Diameter	Retrieval	GPS-Denied/Dark Navigation
DRAGON Zhao et al. (2018)	2017	N	N	N
Quad-Morphing Riviere et al. (2018)	2018	N	N	N
ElbowQuad Devlin et al. (2018)	2018	N	N	N
Foldable Drone Falanga et al. (2019)	2019	N	N	N
Passive Morphing Drone Bucki and Mueller (2019)	2019	N	N	N
SQUID Bouman et al. (2020)	2020	Y	N	N
Ninox 40 MT Paolo Valpolini (2020)	2021	Y	N	N
PowerEgg PowerVision (2023)	2021	Y	N	N
LevelTop LevelTop T1 (2018)	2021	Y	N	N
Spirit Aerosystems (2023)	2022	Y	N	N
Prometheus Titan Brown et al. (2020)	2020	Y	Y	Y

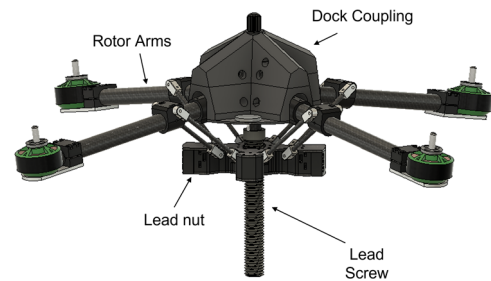
mounted on top of it, which mated with an alignment and latching system on the dock. The latching system used ratchets and paddle wheels to lock the drone in place and to release it.

Chu et al. proposed a vertical dock in 2022, which used electromagnets to lock the drone in place (Chu et al. 2022). Instead of an alignment cone, the drone had a steel plate which adhered to electromagnets in the dock. The drone did not have an upward facing camera, instead the dock had the camera and the drone had an ArUco marker on the steel plate. When the drone is in the field of view of the docking camera, the dock takes control of the drone and guides it into position using visual servoing.

An inverted docking station was proposed in 2020 by De Silva et al. (2022), which used the aerodynamic ceiling effect to adhere the drone to the ceiling before being locked in place by a plate. This system was only designed theoretically, and no prototype system was built.

3 | The Prometheus System

A custom drone was designed and built which met the requirements outlined in Section 1.1. This section presents the specific design features.

**FIGURE 2** | Actuated Aplanar Rotor Arms for the Prometheus Titan II Drone. [Color figure can be viewed at [wileyonlinelibrary.com](https://onlinelibrary.wiley.com/terms-and-conditions)]

3.1 | Titan Drone

The Titan has four aplanar folding arms which are actuated through a central leadscrew as shown in Figure 2. The lead screw is actuated by a motor in the docking mechanism which means that once the robot is undocked, it cannot reconfigure until it re-attaches to the dock itself. This configuration was chosen to reduce the mass of the drone in flight. In the folded configuration, the Titan has a diameter of 130 mm and a vertical length of 660 mm, as shown in Figure 3. When it is unfolded in the flight configuration, it has a tip-to-tip diameter of 815 mm and a vertical length of 545 mm.

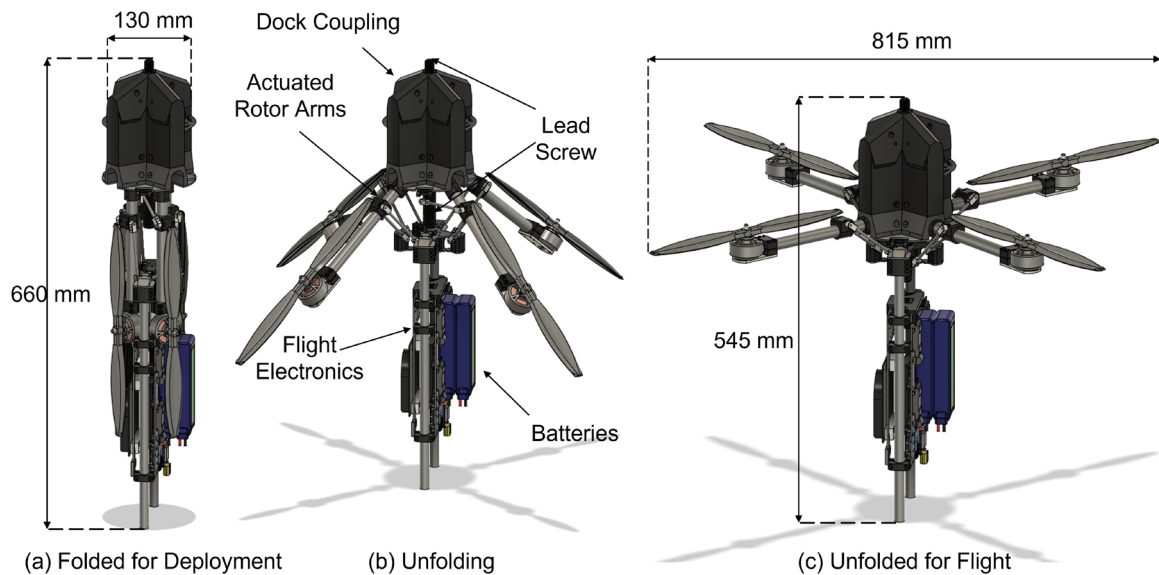


FIGURE 3 | The Prometheus Titan Drone. (a) Folded for Deployment (b) Unfolding (c) Unfolded for Flight. [Color figure can be viewed at [wileyonlinelibrary.com](https://onlinelibrary.wiley.com/doi/10.1002/rob.7012)]

The drone uses an Intel NUC NUC7i7DNKE as the primary data, mapping and path planning processor, which is connected to a Pixhawk 4 flight controller. For sensing and mapping, it uses the Dragonfly sensor system developed by Headlight AI, which is a custom 360° 3D depth sensor package which is mounted at the bottom of the drone. This is formed of an array of IR depth cameras, which have a range of 4 m and provide a field of view of 360° horizontally and 60° vertically. There was also an IR depth camera pointing downward to monitor the distance from objects underneath and the ground itself. Figure 4 shows the fully assembled Prometheus Titan drone. In the final deployment, the drone will not land, so landing skids are not required; however, for ease of use during testing, they were included. The landing skids are not part of the deployment mechanism design and were added for development purposes only.

3.2 | Prometheus Deployment and Docking System

The deployment and docking mechanism is critical for the safe operation of the drone. There are three phases of operation for the system as shown in Figure 5: deployment/retrieval through the borehole, drone reconfiguration, and docking.

In the deployment/retrieval phase, the drone is in the folded position and is secured inside a protective case to stop it from being damaged by loose or sharp material inside the borehole (Figure 5a). Once it has reached the end of the borehole and has exited into the cave void, there are two issues to address. The first is that the deployment mechanism so has to act as a stable launch platform. To do this, an active wall pressing assembly, based on the concepts developed for pipe inspection robots (Brown et al. 2021), was integrated. When activated, this is used to stabilize the dock inside the borehole by applying pressure to the walls of the borehole. The deployment mechanism with the wall pressing assembly is 625 mm long and has a diameter of 140 mm.

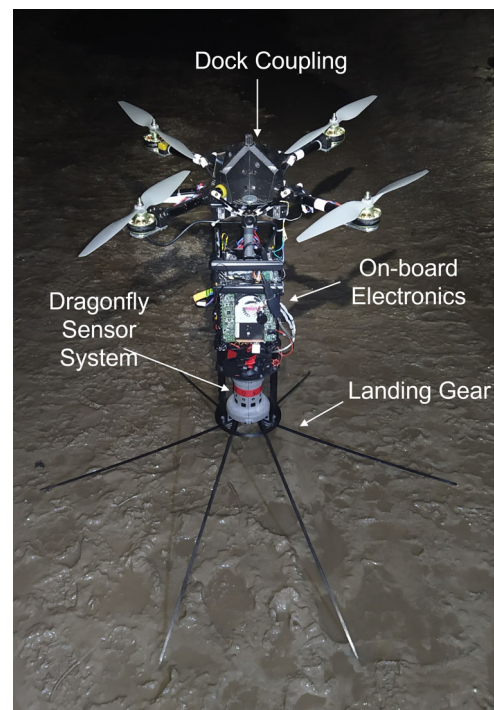


FIGURE 4 | The Prometheus Titan Drone in a Test Configuration with Temporary Landing Gear. [Color figure can be viewed at [wileyonlinelibrary.com](https://onlinelibrary.wiley.com/doi/10.1002/rob.7012)]

The second consideration is the alignment of the dock. Boreholes can be drilled up to 10° from the vertical, whereas launch and, in particular, recovery of the drone is most easily achieved with the docking mechanism aligned with the vertical. To overcome this, the dock is on a universal pivot joint, which uses the mass of the drone to angle the dock to the vertical plane before launch and the subsequent recovery.

Once the drone has exited the borehole, it needs to be re-configured into flight mode through the central lead screw system as described in Section 3.1. Figure 6 shows the dock,

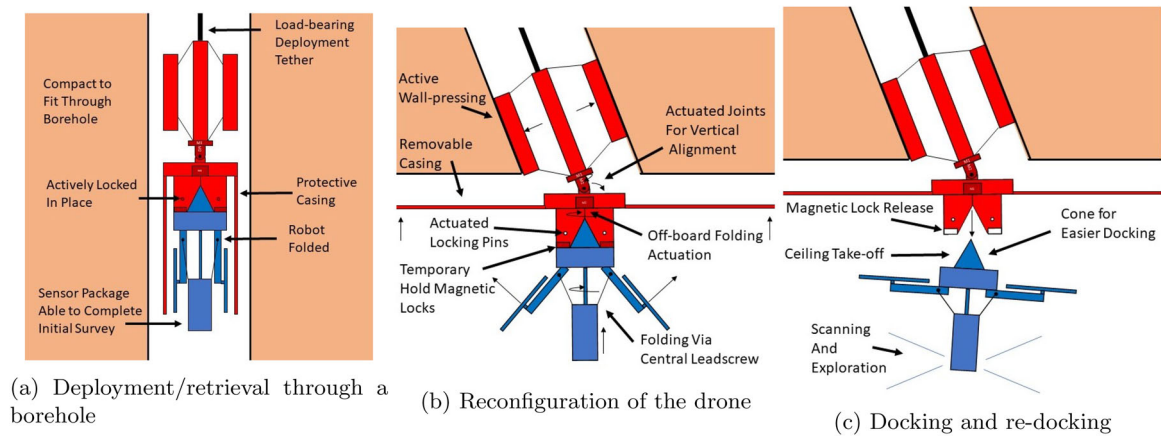


FIGURE 5 | Key Design Features of the Deployment Mechanism and Robot (Brown et al. 2020). (a) Deployment/retrieval through a borehole, (b) Reconfiguration of the drone, (c) Docking and re-docking. [Color figure can be viewed at [wileyonlinelibrary.com](https://onlinelibrary.wiley.com/doi/10.1002/rob.70112)]

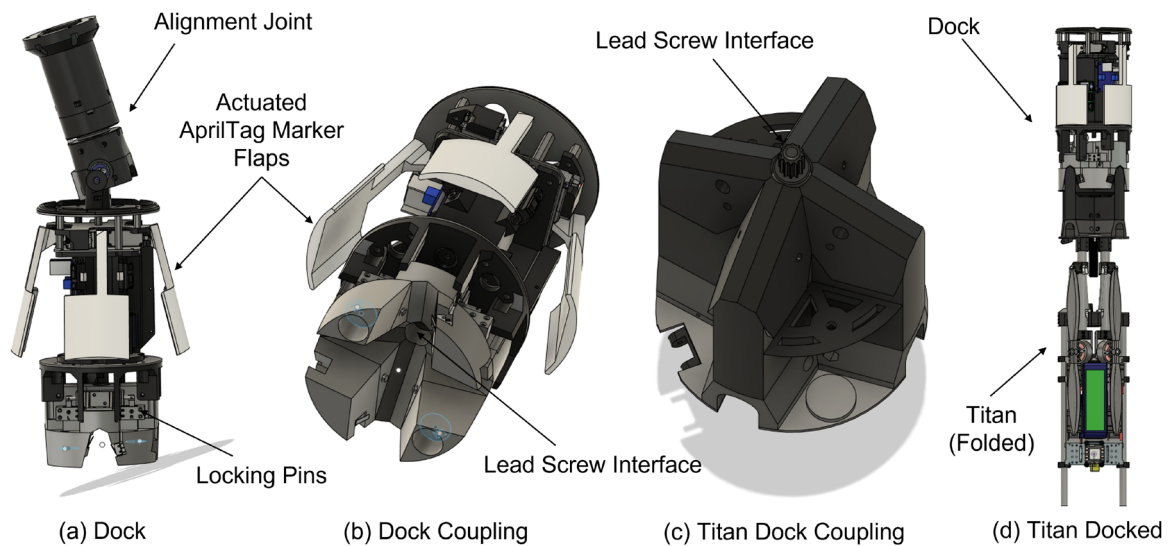


FIGURE 6 | Docking System. (a) Dock (b) Dock Coupling (c) Titan Dock Coupling (d) Titan Docked. [Color figure can be viewed at [wileyonlinelibrary.com](https://onlinelibrary.wiley.com/doi/10.1002/rob.70112)]

with the alignment joint and the lead screw interface for both the dock and the Titan. Once in the flight configuration, the drone can be deployed.

The drone is held in the dock through the combination of a magnetic lock and actuated locking pins. To launch the drone, the flight system is activated so that the drone is in hover mode and the propellers are spun up to flight speed for the hover, whilst it is still fixed into the dock. The locking pins and magnetic lock are then released, and the drone is automatically commanded to move to a position just below the dock and hover in place, ready for a mission to start.

3.3 | Prometheus Control and Docking

To re-dock, the drone's mission planner sets a waypoint just underneath the dock for it to hover. Once positioned, an upward-facing camera identifies AprilTags, which are deployed on small actuated arms from the dock. Using

visual servoing, the drone aligns itself both in translation and rotation using the AprilTags as reference points. Once the drone coupling mechanism (Figure 6c) has engaged with the dock (Figure 6b), the connection is confirmed by an IR sensor in the dock and the locking pins are activated which physically secure the drone. Figure 7 shows the full deployment and docking system with the drone attached.

The use of AprilTags on actuated arms allows the docking mechanism itself to be centrally located. Furthermore, the greater diameter between them once deployed improves the position estimation of the dock for the drone when in flight. The docking process takes place relatively slowly, with the local set-point for flight control moving from the hover point up toward the capture mechanism. Due to the subterranean location, the only movement of air locally is due to the drone itself, and so the aerodynamic effects are predictable and repeatable. Because the docking mechanism protrudes through the ceiling of the void to allow it to align with the vertical, the ceiling effect was found to be minimal.

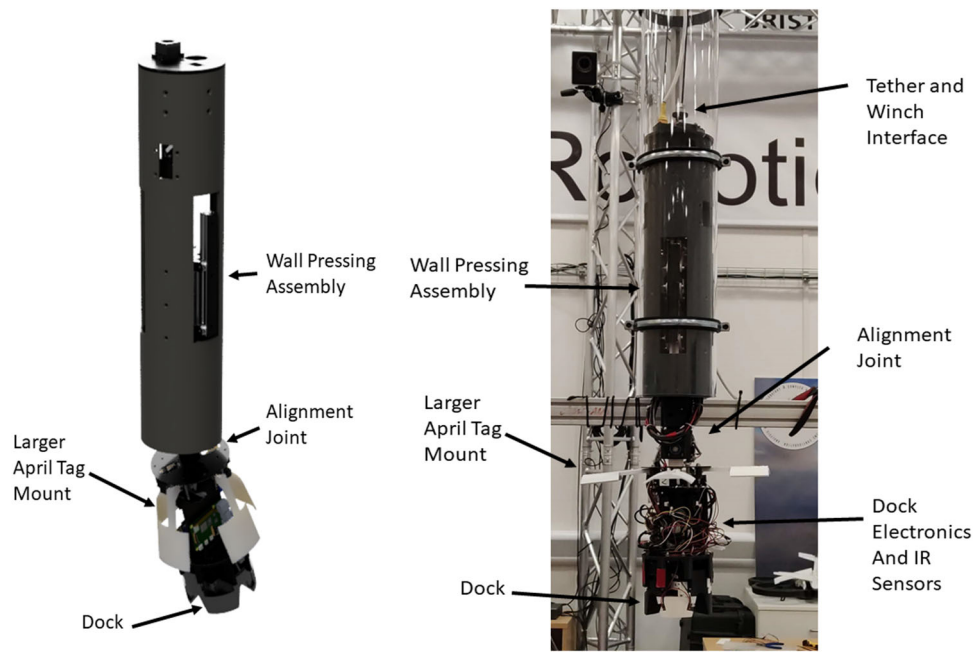


FIGURE 7 | Prometheus Deployment Mechanism. [Color figure can be viewed at [wileyonlinelibrary.com](https://onlinelibrary.wiley.com/doi/10.1002/rob.7012)]

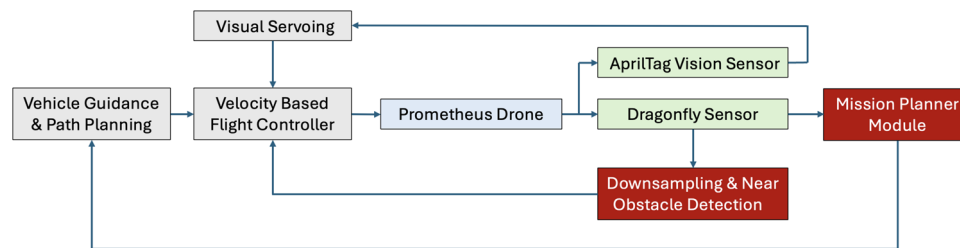


FIGURE 8 | Prometheus Titan Control System Architecture showing Inner Loop Obstacle Avoidance with Outer Loop Mapping, Mission and Path Planning. [Color figure can be viewed at [wileyonlinelibrary.com](https://onlinelibrary.wiley.com/doi/10.1002/rob.7012)]

Once the drone makes contact with the dock, the control system has been designed to apply positive upward pressure on the mechanism until the locking pins have been deployed. At this point, the drone is powered down, the AprilTags are folded up, and the motor on the dock is used to fold down the drone rotor arms before retrieval. The wall pressing arms are subsequently released, and the whole Prometheus system is withdrawn using a pulley from above, with the mechanical effect of the borehole aligning the dock with the upper assembly as it exits from the void.

In flight, the Dragonfly sensor system is used to provide data for localization, mapping, and path planning computation as well as faster rate data for position and velocity-based flight control. There is a considerable amount of data generated in real-time through the Dragonfly sensor, and so for the lower-level control to ensure separation from the walls of the void, this is sampled and used to provide simple proximity sensing. This is carried out relatively quickly in a separate software module with the mission planner running at a much lower frequency. The drone is stabilized relative to the immediate surroundings through the use of a velocity-based controller with the outer loop providing navigation through the void based on the lower rate path planning, SLAM-based estimations.

The Mission Planner module is required to maintain a minimum distance to the closest obstacles in its vicinity for the paths that are generated, however, it was found in practice that the best results were obtained with running this in parallel with a fast response inner-loop velocity controller based on down-sampled data from the Dragonfly. This provided a quick response to uncertainties and disturbances in the environment whilst complementing the in-depth mapping and planning in the outer loop (Figure 8).

For the purposes of these field demonstrations, the maximum lateral flight speed was limited to 1.0 m/s along all axes, which allowed for relatively precise location estimates and ample time to react to the presence of obstacles and for re-planning. Even with a limited flight time of 10 min, this allows for an exploration distance of over 150 m with a 4-min flight time budget for launch and recovery. Further development of the system with a reduction in flight mass and an increase in the maximum horizontal flight speed could significantly increase this range. Within the field trials, fully autonomous deployment, recovery and flight within an unknown void were all demonstrated, with the only additional sensors required being the Dragonfly system and an upward-facing camera. It should be noted that, for the purposes of the field trials, ambient light was provided for

locating the AprilTag sensors. During operation, this light would need to be provided by the Prometheus system itself, or an alternative location sensor would need to be used for the approach to docking.

4 | Mission Planning

For the Prometheus drone, a mission planner was developed that addresses the challenge of making inspection tasks tractable while maximizing the acquisition of information about the environment, all while ensuring safety. The approach taken encompasses both navigation planning and exploration planning in parallel, as depicted in Figure 9. By combining these two elements, the planner generates feasible paths and constructs a comprehensive 3D occupancy map of the largest available space.

4.1 | Navigation Planning

Navigation planning is a crucial component of the mission planner, focusing on generating collision-free paths for the robot. To achieve this, a version of a sampling-based motion planning algorithm was developed that is capable of planning under incomplete information about the robot's workspace (Akbari and Bernardini 2021a). This algorithm incorporates a re-planning capability (Akbari et al. 2020).

The motion planning algorithm generates a path consisting of a set of waypoints, ensuring that each point is collision-free. Initially, with limited information about the free and occupied space in the robot's workspace, the algorithm plans a path based on the available data. As the robot starts following the path and captures more information through its sensors, this new information is fed back into the planning process.

This feedback loop enables the robot to evaluate the collision-free status of the remaining waypoints in the path. If any collisions are detected, the re-planning process is triggered, resulting in the generation of a new path from the current waypoint. This iterative approach ensures that the robot can adapt to dynamically changing environments and avoid potential obstacles or hazards.

To further enhance safety during navigation, the planner is equipped with a cost function. This function ensures that the robot maintains a minimum distance between its position and

the closest obstacles in its vicinity. By incorporating this safety measure, the robot can confidently navigate to new areas while minimizing the risk of collisions. Figure 10 provides an illustrative example of the navigation of a drone within a confined space, while effectively adhering to the safety distance from the obstacles. The planner dynamically computes collision-free paths for the robot, ensuring that it stays within a safe range from the obstacles present in the environment.

Additionally, the navigation planner addresses the requirement of the robot safely returning to its home position when its battery is running low. By utilizing the navigation planner, the robot can plan a collision-free path back to the home position, ensuring a safe return even under limited battery power. It should be noted that for the flight tests that are shown in Figure 10, the Vicon sensors that can be seen in the background of the image were used as a surrogate sensor in place of the Dragonfly for the purposes of testing the planner for flight in a representative constriction.

Overall, all these features collectively contribute to the safe and efficient navigation of Prometheus during its missions. The initial flight tests at the Bristol Robotics Laboratory shown in Figure 10 were used to test the speed and reliability of the planner with uncertainty created in the environment through movement of the artificial cave between each of the test runs. The constriction shown in this image was also purposefully designed to be smaller than those that Prometheus was tested on the field and shown later in this paper.

4.2 | Exploration Planning

An advanced and informed exploration planning algorithm was developed to efficiently guide the robot's exploration task (Akbari and Bernardini 2021a) while simultaneously constructing a comprehensive 3D occupancy map of the environment. This algorithm consists of two primary components: the reachability graph and the utility function.

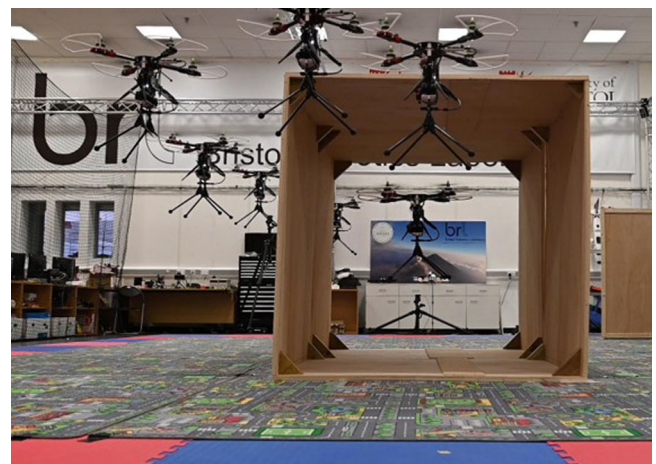


FIGURE 10 | Prometheus Titan Navigation through an Artificial Cave at the Bristol Robotics Laboratory, Adhering to its Safety Distance proposed by the Navigation Planner. [Color figure can be viewed at [wileyonlinelibrary.com](https://onlinelibrary.wiley.com/doi/10.1002/rob.70112)]

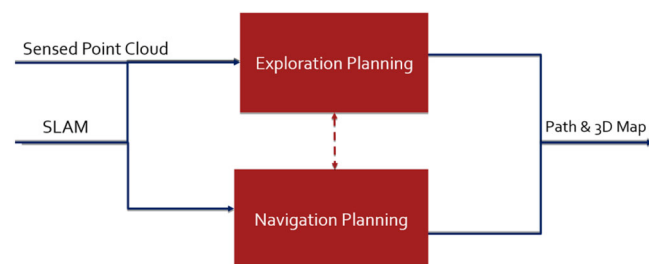


FIGURE 9 | Prometheus Titan Mission Planner Module Architecture. [Color figure can be viewed at [wileyonlinelibrary.com](https://onlinelibrary.wiley.com/doi/10.1002/rob.70112)]

The mission planner incorporates a dynamic reachability graph, where vertices and edges are generated as the robot explores the environment. As the robot executes a motion plan using the navigation planner, the mission planner creates vertices along the planned path and identifies frontier nodes, which exist between known and unknown areas, from each vertex. Subsequently, edges are established between pairs of vertices, forming the reachability graph.

To manage the complexity associated with the frontier nodes, a subset of frontier voxels is sampled. This sampling process aims to reduce computational overhead whilst ensuring that the system can perform various calculations based on the frontier. To achieve this, a minimum distance, denoted as d_s , is selected as a threshold between two samples. If the distance between a candidate sample and any of the previously chosen samples is less than d_s , the candidate is discarded. This selection criterion helps maintain diversity among the sampled frontier voxels.

To ensure that the selected candidates are geometrically feasible, a collision detection module is employed. This module verifies whether the candidates are free from collisions with obstacles or other objects in the environment. By incorporating this collision detection mechanism, the planner guarantees that the generated samples align with the physical constraints of the robot and the environment, promoting safe and reliable exploration.

The sampling mechanism employed by the mission planner takes into account the specific type of region in which the robot is currently exploring. This adaptability is crucial for optimizing the sampling process based on the characteristics of the environment. To determine the type of region, a ray-casting method is utilized, which evaluates whether the robot is situated in a narrow passage or a void region.

When the robot is navigating through a narrow region, the sampling process is biased toward considering frontier voxels located in the centre of the area. This bias ensures that the samples are more focused on exploring the critical parts of the narrow passage. On the other hand, when the robot is exploring a void area, the sampler takes into account the entire frontier set. This approach allows for a broader exploration of the void region, maximizing the coverage and potential information acquisition in these unexplored regions.

The density of the sampling is determined based on the information available in the reachability graph. Given a specific vertex, denoted as v , the sampler identifies the neighboring vertices of v and samples the frontiers using these neighboring vertices as references. This strategy leverages the reachability graph's information to guide the sampling process and ensure that the samples are representative and diverse.

A utility function has been devised to facilitate the selection of the most advantageous sampled frontier node for the robot to visit during the exploration process. This utility function incorporates three essential factors: information gain, safety constraints, and path length, enabling a comprehensive evaluation of each candidate. To quantify the information gain, Shannon's entropy (Gray 2011) is employed, a well-established

measure of uncertainty in information theory. This approach allows us to assess the level of information contained within a selected sampled frontier candidate. The *utility function* $U(.)$ of a frontier node s is defined in Equation (1).

$$U(s) = \delta \mathcal{H}(s) \exp(-\gamma L(s))(1 + \zeta D) \quad (1)$$

where $\mathcal{H}(.)$ is the entropy function that returns a numeric value indicating how much new information can be obtained by visiting node s . $L(.)$ is the length of the path from the initial position to node s , D is the safety distance, and δ , γ , and ζ are tuneable parameters.

The entropy function $\mathcal{H}(s)$ quantifies how much new information can be gained by visiting a given node s . It is based on Shannon's entropy (Gray 2011), which measures the expected information gain associated with an observation. In our context, this is achieved by analyzing the occupancy probabilities of voxels in the 3D map, specifically the likelihood of each voxel being free, occupied, or unknown. Regions with higher uncertainty result in higher entropy values, reflecting a greater potential for information gain. This formulation enables the robot to prioritize frontier nodes that are more likely to lead to unexplored areas of the environment during autonomous exploration.

The safety distance D is defined as the distance between a candidate node s and the nearest occupied voxel in the 3D occupancy map. This constraint ensures that the robot maintains a minimum buffer from obstacles, allowing for safe navigation during exploration. The value of D is determined based on the robot's physical size and motion characteristics, ensuring that it can operate without risk of collision when moving toward unexplored areas.

The utility function parameters δ , γ , and ζ can be tuned according to the challenges of the different scenarios to give more or less importance to the various part of the utility function, which combines the total information gain with safety distance D from the obstacles and length of the motion. Higher values for ζ were chosen when the robot navigates within narrow areas than when it is moving in void spaces to maintain the robot in the centre of the region. Additional details on the parameters and the utility function in general can be found in the authors' previous work (Akbari et al. 2020; Akbari and Bernardini 2021b).

Once the best frontier candidate has been selected based on the utility function evaluation, the mission planner proceeds to call the navigation planner to generate a motion plan. This motion plan outlines the specific path that the robot should follow to reach the selected frontier node. Before executing the motion plan, the mission planner verifies whether the robot has sufficient battery power to complete the planned trajectory. If there is not enough battery available, the robot aborts the execution of the motion plan and safely returns to the home position. Conversely, if the robot has adequate battery capacity, it proceeds to execute the motion plan, allowing the robot to traverse the planned trajectory and reach the selected frontier node.

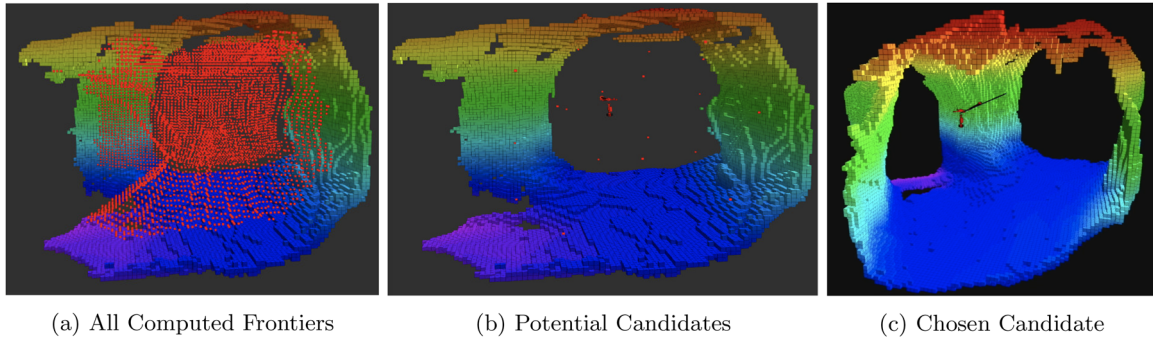


FIGURE 11 | Frontier nodes, represented by voxels, are computed whenever the robot arrives in a target node. Potential frontier nodes are then chosen based on the utility value from Equation (1). From these nodes, one is sampled to be the target node s , which will drive the robot to reach the node. (a) All Computed Frontiers, (b) Potential Candidates, (c) Chosen Candidate. [Color figure can be viewed at [wileyonlinelibrary.com](https://onlinelibrary.wiley.com/doi/10.1002/rob.70112)] [wileyonlinelibrary.com](https://onlinelibrary.wiley.com/doi/10.1002/rob.70112)]

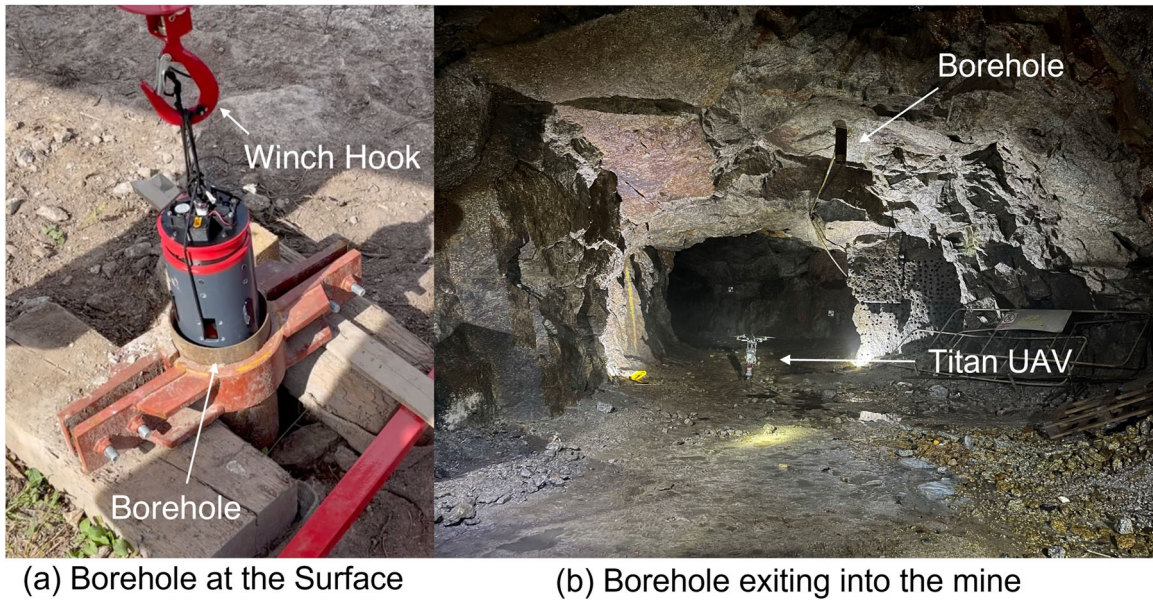


FIGURE 12 | Borehole from Surface to Cavern. (a) Borehole at the Surface (b) Borehole exiting into the mine. [Color figure can be viewed at [wileyonlinelibrary.com](https://onlinelibrary.wiley.com/doi/10.1002/rob.70112)] [wileyonlinelibrary.com](https://onlinelibrary.wiley.com/doi/10.1002/rob.70112)]

As shown in Figure 11, the frontier voxels are visually represented that have been computed during an exploration task, along with the corresponding sampled frontier candidates. These candidates represent potential locations that the robot can visit to gather new information about the environment.

To determine the most promising candidate to visit next, the exploration planner invokes the utility function for each of these candidates. The utility function evaluates and assigns a value to each candidate based on its information gain, safety constraints, and path length. This evaluation allows for a quantitative comparison of the candidates, enabling the selection of the candidate with the highest utility value.

5 | Real World Experiments

The Prometheus system was deployed in Holman's test mine, UK, in July 2021. The mine is an old granite quarry which has over 2 km of tunnels over a 0.12 km² site. A borehole was

commissioned for deployment of the drone from the surface as shown in Figure 12. The borehole was 150 mm in diameter and 19 m in length. An unforeseen challenge with the borehole was water ingress. Once it had been drilled, there was a significant amount of water seeping from the ground and rock. The Titan prototype was not built to be waterproof, so a liner and hosepipe arrangement had to be inserted into the borehole to reduce the amount of water flowing out of the hole.

5.1 | Docking and Re-Docking

On the surface, the drone was deployed via a winch system, shown in Figures 12a and 13a. The deployed dock and unfolded Titan drone are shown in Figure 13b. The video <https://youtu.be/fiGmgJKaU34> shows the successful launching of the drone from the dock. Once it has been released from the locking pins, it descends to a predetermined height and hovers before progressing with the mission.

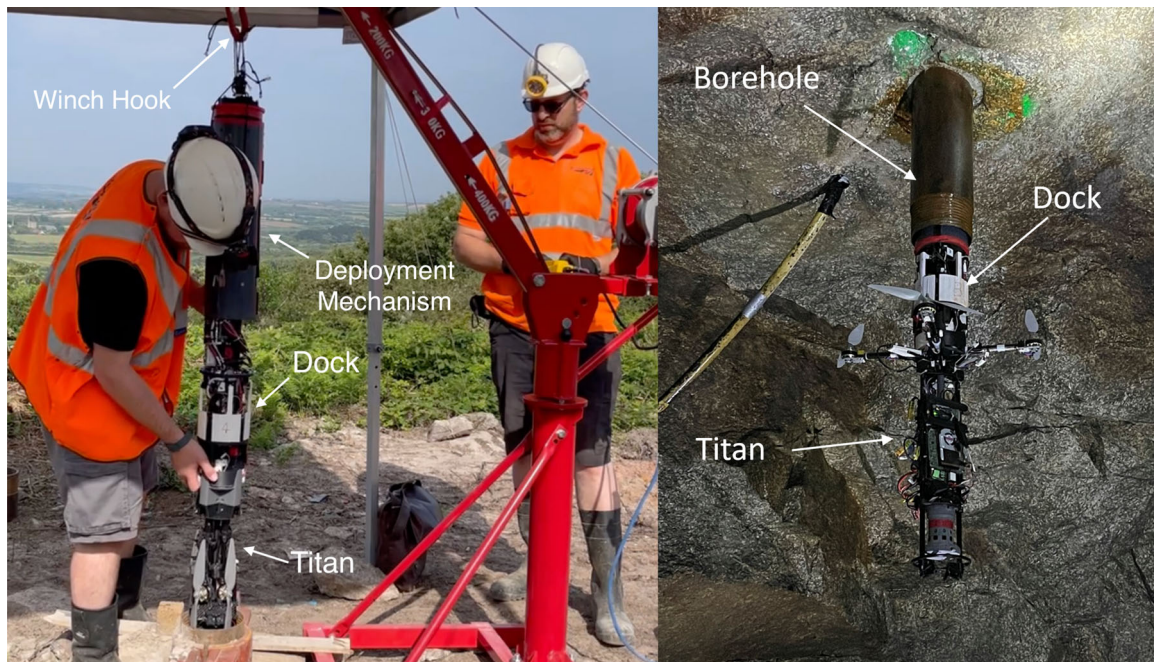


FIGURE 13 | Deployment of the Titan drone through the borehole. [Color figure can be viewed at [wileyonlinelibrary.com](https://onlinelibrary.wiley.com/doi/10.1002/rob.7012)] [wileyonlinelibrary.com](https://onlinelibrary.wiley.com/doi/10.1002/rob.7012)]

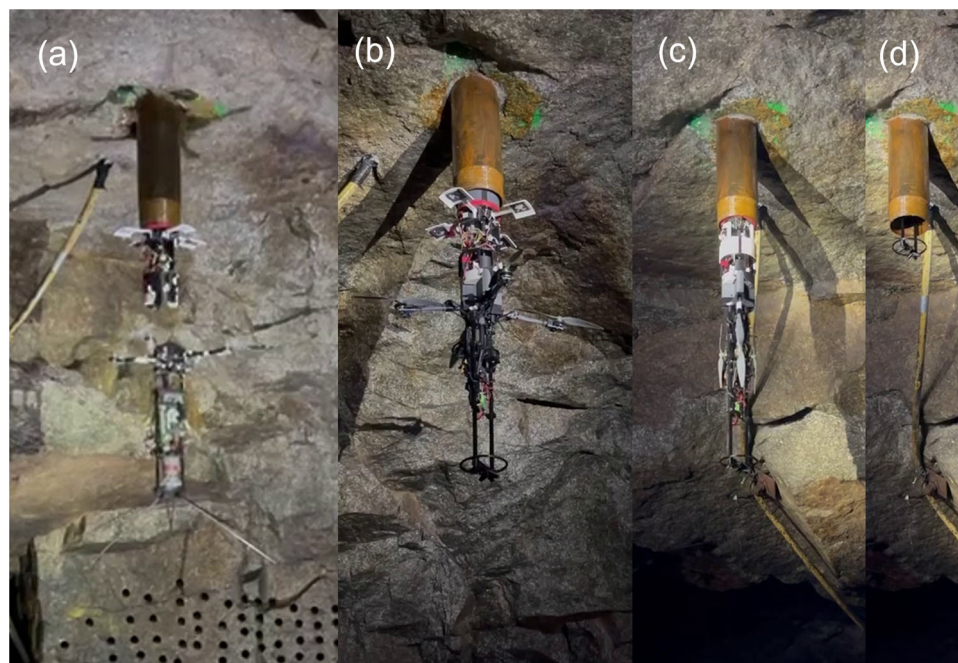


FIGURE 14 | Titan Re-docking Process (a) Switching to Visual Servoing; (b) Docking; (c) Reconfiguring into Folded Mode and (d) Retrieval up the Borehole. [Color figure can be viewed at [wileyonlinelibrary.com](https://onlinelibrary.wiley.com/doi/10.1002/rob.7012)] [wileyonlinelibrary.com](https://onlinelibrary.wiley.com/doi/10.1002/rob.7012)]

Once the mission has been completed, the re-docking process is triggered. Figure 14 shows the individual stages; (a) the drone hovers underneath the dock and switches to visual servoing for accurate positioning. (b) shows the drone moving vertically toward the dock and engaging with the coupling system. In (c) and (d), the drone has successfully docked and is folded back into the compact form before it is winched back up the borehole to the surface. Both the launching and the re-docking processes were fully automated with no human input once they had been started. It should be noted that the figure here is a composite

with images taken from different flights and system configurations. To reduce risk to the vehicle during the field trials, temporary landing legs were installed whilst the aircraft was undocking and in flight to allow for a conventional landing should it be required during testing.

Prolonged explorations often lead to accumulated localization errors. In our trial, we tackled this issue through a combination of limiting the maximum lateral flight speed to 1.0 m/s, providing larger AprilTag sensors on the mounting system, and



FIGURE 15 | Flying in the Tunnels. [Color figure can be viewed at [wileyonlinelibrary.com](https://onlinelibrary.wiley.com/doi/10.1002/rob.7012)]

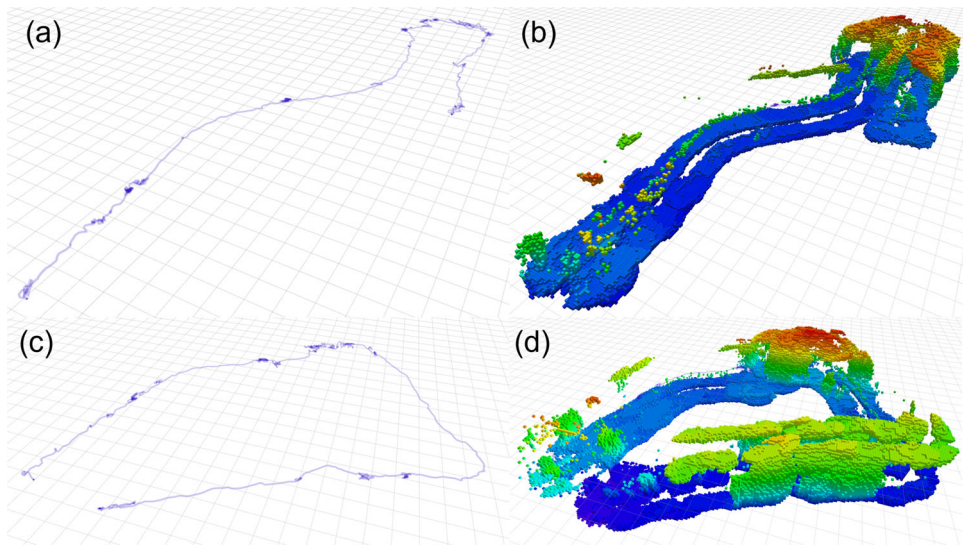


FIGURE 16 | Maps Generated from Flights (a) Path of Flight 1; (b) Octomap of Flight 1; (c) Path of Flight 2 and (d) Octomap of Flight 2. [Color figure can be viewed at [wileyonlinelibrary.com](https://onlinelibrary.wiley.com/terms-and-conditions)]

providing ambient light surrounding the AprilTags. We managed to minimize accumulation errors with the average flight time of 10 min to an acceptable localization level, where the Prometheus drone was still able to identify the tags with its upward-facing camera.

5.2 | Confined Space Flights

Whilst the docking processes were automated, a fully autonomous end-to-end flight in the mine was not possible due to the time restrictions of the project. Each individual component of a whole mission was demonstrated and manually directed flights were undertaken to (a) observe the flight dynamics of the drone in confined spaces (b) gather data to assess the performance of the sensing system and (c) generate data sets which could be used to create digital twins and simulation environments for

future development. During these flights, the Dragonfly sensor was being used to map the environment and produce the reduced data set for the flight controller to do real-time obstacle avoidance with a pilot supplying higher level velocity commands. This means that the input to the flight controller was a simple direction and speed command, with the lower level sensing and control of the vehicle being carried out automatically. Figure 15 shows the Titan drone being flown through one of the tunnels.

The supporting video <https://youtu.be/fiGmgJKaU34> shows footage of the flight through some of the tunnels. One of the key observations from the flights was the effect of turbulence from wall, ceiling, and ground effects on the stability of the drone. During deployment and re-docking, this was not found to have a significant impact, in particular because the docking controller had been tested and tuned extensively at the Bristol

Robotics Laboratory in a variety of different configurations. Wall effects, however, were found to be relatively significant, and follow-on work with this project would include additional control system development focused on close-proximity flying in confined areas.

The in-flight mass of the Prometheus drone as flown in these field trials was approximately 3 kg. Because of this, the motor and propeller configuration was relatively highly loaded. Driven primarily by the overall sensor and computing requirements, both the flying properties, endurance, and overall system performance would benefit significantly from a reduction in payload and the associated overall flying mass.

With autonomous deployment and recovery and manually guided flights, data was captured for different sections of the test tunnels. Figure 16 shows examples of the maps generated from the tunnels, with (a) and (c) presenting sections of the paths flown, and (b) and (d) providing a partial visualization of the tunnel walls associated with these two paths. The relative length of both paths is in the region of 100 m. Stabilization and obstacle avoidance for these flights were both provided in real-time onboard the vehicle, with the automated exploration being demonstrated offline with the captured data sets and in the test facility at the Bristol Robotics Laboratory.

6 | Conclusions and Further Work

This paper presents the final configuration and field trials of the Prometheus drone, which was an Innovate UK-funded project to develop a system for the exploration of access-restricted voids. The final field trials at Holman's test mine demonstrated ingress and egress through a 150 mm borehole with automated deployment and recovery of the drone from a bespoke release and capture mechanism.

Robust flight using visual time-of-flight (ToF) sensors was also demonstrated with parallel onboard mapping using the Dragonfly sensor. Exploration and Navigation algorithms have been developed to efficiently explore three-dimensional spaces whilst ensuring separation from obstacles. These algorithms have also been run onboard the Prometheus drone with real-time demonstrations carried out in the Bristol Robotics Flight Arena.

Follow-up work on this project is currently being planned, which is focused on three key areas. The first of these is a reduction in overall mass of the vehicle; the second is a reduction in the complexity of the sensors; and the third is a future set of trials to take the system through to full autonomy. Since the trials covered in this paper, the platform itself has been further developed by Callen-Lenz and Headlight AI, details of which can be found at: <https://callenlenz.com/platforms>.

The payload of any air vehicle drives the overall flight mass, which, in the case of the Prometheus Titan drone, was a payload of approximately 1 kg, leading to an overall mass of just over 3 kg. This payload fraction is slightly lower than comparison vehicles due to the added mass introduced by the folding mechanism for deployment and recovery. With the payload

primarily consisting of the Dragonfly sensor, compute and associated power systems, if this is reduced significantly, it would lead to a significant reduction in overall flight mass, together with associated improvements in performance. Additional mass could also be used to improve the robustness of the system.

Currently, the Dragonfly sensor generates very high data rates due to the multiple ToF sensors placed around the central ring. Future work will enhance efficiency by reducing compute and power requirements, which can be achieved by limiting the scan frequencies, number, and type of these sensors. There is a balance between simplicity for the inner loop control and obstacle avoidance and the need for a rich data environment for mapping and mission planning. With an overall aim to reduce the in-flight mass by two-thirds, future Prometheus flight demonstrators will provide a step change in performance and robustness whilst continuing to meet the automated mapping and planning requirements.

The third key area for future development and flight tests is additional integrated tests leading to full autonomy. Each capability of the Prometheus systems was developed and demonstrated individually in the flight lab, however real-world tests introduce uncertainty and complexity and therefore make end-to-end demonstrations more challenging. Future development tests within the Prometheus Titan drone are being designed to build up the complexity of simple complete end-to-end missions as opposed to bringing together fully formed complex capabilities. Simple demonstrations will be employed, leading on to full autonomous exploration of the Holman's test mine.

Finally, the fourth key area for future development is addressing potential accumulated localisation errors. In our experiments, limiting the flight speed and providing larger AprilTag sensors was sufficient to tackle the localization errors when docking the drone back at the mounting system. However, prolonged explorations of longer than 10 min might have increased the errors significantly. We plan to tackle this issue by combining shorter explorations with planned return paths, performing periodic map corrections, and utilizing artificial landmarks. Exploration paths that naturally loop back toward known areas will be created, with artificial landmarks. Every time the drone uncovers a new area, it marks the area with an artificial marker generated from the Dragonfly (e.g., sharp edges of a split path). It continues to visit this new area to provide an estimated position of where the artificial marker was placed, which can in turn be corrected by the base station.

In conclusion, the fundamental design concept as embodied by the Prometheus drone has the potential to meet the access requirements as identified by Network Rail Infrastructure Limited. There is also a wide range of additional applications where this capability would be of significant benefit. Further work is required to realize the full potential of the overall system. Future refinements will also reduce size, weight, and system complexity whilst retaining the mapping capabilities needed. There is still an open ended question as to whether a multi-modal vehicle might be necessary for some of the exploration envisaged by the end user, however, the potential of

the Prometheus drone with deployment through a 150 mm borehole has been clearly demonstrated.

Acknowledgments

This study has been completed in partnership with the following companies that have provided insight and technical expertise to the project: Callen-Lenz, Headlight AI Limited, Network Rail Infrastructure Limited and Thales UK Limited. Prometheus (104824) was funded through the Industrial Strategy Challenge Fund under the Robotics and AI in Extreme Environments challenge. The Industrial Strategy Challenge Fund is delivered by UK Research and Innovation. It was also funded by the Robotics and AI Hub (RAIN Hub) EP/R026084/1.

Data Availability Statement

The data that support the findings of this study are available on request from the corresponding author. The data are not publicly available due to privacy or ethical restrictions.

References

- Aerosystems, A. 2023. Spirit. Ascent AeroSystems. <https://ascentaerosystems.com/spirit/>.
- Agha, A., K. Otsu, B. Morrell, et al. 2022. "Nebula: Team CoSTAR's Robotic Autonomy Solution That Won Phase II of Darpa Subterranean Challenge." In *Field Robotics*, Vol.2, 1432–1506. <https://doi.org/10.55417/fr.2022047>.
- Akbari, A., and S. Bernardini. 2021a. "Informed Autonomous Exploration of Subterranean Environments." *IEEE Robotics and Automation Letters* 6, no. 4: 7957–7964.
- Akbari, A., and S. Bernardini. 2021b. "Informed Autonomous Exploration of Subterranean Environments." *IEEE Robotics and Automation Letters* 6, no. 4: 7957–7964.
- Akbari, A., P. S. Chhabra, U. Bhandari, and S. Bernardini. 2020. "Intelligent Exploration and Autonomous Navigation in Confined Spaces." In *2020 IEEE/RSJ International Conference on Intelligent Robots and Systems (IROS)*, 2157–2164. IEEE.
- Azpúrua, H., M. Saboia, G. M. Freitas, et al. 2023. "A Survey on the Autonomous Exploration of Confined Subterranean Spaces: Perspectives From Real-World and Industrial Robotic Deployments." *Robotics and Autonomous Systems* 160: 104304.
- Azpúrua, H., A. Rezende, G. Potje, et al. 2021. "Towards Semi-Autonomous Robotic Inspection and Mapping in Confined Spaces With the Espeleorob." *Journal of Intelligent & Robotic Systems* 101: 69. <https://doi.org/10.1007/s10846-021-01321-5>.
- Bouman, A., P. Nadan, M. Anderson, et al. 2020. "Design and Autonomous Stabilization of a Ballistically-Launched Multirotor." In *2020 IEEE International Conference on Robotics and Automation (ICRA)*, 8511–8517. IEEE.
- Brown, L., J. Carrasco, and S. Watson. 2021. "Autonomous Elbow Controller for Differential Drive In-Pipe Robots." *Robotics* 10, no. 1: 28. <https://doi.org/10.3390/robotics10010028>.
- Brown, L., R. Clarke, A. Akbari, et al. 2020. "The Design of Prometheus: A Reconfigurable UAV for Subterranean Mine Inspection." *Robotics* 9, no. 4: 95. <https://doi.org/10.3390/robotics9040095>.
- Bucki, N., and M. W. Mueller. 2019. "Design and Control of a Passively Morphing Quadcopter." In *2019 International Conference on Robotics and Automation (ICRA)*, 9116–9122. IEEE.
- Cheah, W., K. Groves, H. Martin, et al. 2023. "Mirrax: A Reconfigurable Robot for Limited Access Environments." *IEEE Transactions on Robotics* 39, no. 2: 1341–1352.
- Cheng, C., X. Li, L. Xie, and L. Li. 2022. "Autonomous Dynamic Docking of Uav Based on UWB-Vision in GPS-Denied Environment." *Journal of the Franklin Institute* 359, no. 7: 2788–2809.
- Chu, P. -H., Y. T. Huang, C. -H. Pi, and S. Cheng. 2022. "Autonomous Landing System of a Vtol Uav on an Upward Docking Station Using Visual Servoing." *IFAC-PapersOnLine* 55, no. 27: 108–113.
- DARPA. 2020. *Darpa Subterranean Challenge Competition Rules Cave Circuit*. Technical Report, Defense Advanced Research Projects Agency. https://www.darpa.mil/sites/default/files/SubT_Challenge_Finals_Rules.pdf.
- De Silva, S. C., M. Phlernjai, S. Rianmora, and P. Ratsamee. 2022. "Inverted Docking Station: A Conceptual Design for a Battery-Swapping Platform for Quadrotor Uavs." *Drones* 6, no. 3: 56. <https://doi.org/10.3390/drones6030056>.
- Deng, L., B. Yang, X. Dong, et al. 2023. "Self-Spin Enabled Docking and Detaching of a UAV-UGV System for Aerial-Terrestrial Amphibious and Independent Locomotion." *IEEE Robotics and Automation Letters* 8, no. 5: 2454–2461.
- Devlin, T., R. Dickerhoff, K. Durney, et al. 2018. ElbowQuad: Thrust Vectoring Quadcopter. <https://doi.org/10.2514/6.2018-0893>.
- Falanga, D., K. Kleber, S. Mintchev, D. Floreano, and D. Scaramuzza. 2019. "The Foldable Drone: A Morphing Quadrotor That Can Squeeze and Fly." *IEEE Robotics and Automation Letters* 4, no. 2: 209–216.
- Galimov, M., R. Fedorenko, and A. Klimchik. 2020. "UAV Positioning Mechanisms in Landing Stations: Classification and Engineering Design Review." *Sensors* 20, no. 13: 3648. <https://doi.org/10.3390/s20133648>.
- Gray, R. M. 2011. *Entropy and Information Theory*. Springer Science & Business Media.
- Grlij, C. G., N. Krznar, and M. Pranjić. 2022. "A Decade of UAV Docking Stations: A Brief Overview of Mobile and Fixed Landing Platforms." *Drones* 6, no. 1: 17. <https://doi.org/10.3390/drones6010017>.
- Hudson, N., F. Talbot, M. Cox, et al. 2022. "Heterogeneous Ground and Air Platforms, Homogeneous Sensing: Team CSIRO Data61's Approach to the DARPA Subterranean Challenge." *Field Robotics* 2: 595–636. <https://doi.org/10.55417/fr.2022021>.
- Krátký, V., P. Petráček, T. Báča, and M. Saska. 2021. "An Autonomous Unmanned Aerial Vehicle System for Fast Exploration of Large Complex Indoor Environments." *Journal of Field Robotics* 38, no. 8: 1036–1058.
- Leveltop T1. 2018. Quick Start Guide V1.1. LevelTop Technology, Tech Report 2018. <https://fcc.report/FCC-ID/2AR2U-T1/4128409.pdf>.
- Lieret, M., F. Wurmer, C. Hofmann, and J. Franke. 2021. "An Overhead Docking and Charging Station for Autonomous Unmanned Aircraft." In *2021 IEEE 17th International Conference on Automation Science and Engineering (CASE)*, 1358–1363. IEEE.
- Lindqvist, B., C. Kanellakis, S. S. Mansouri, A. Akbar Aghamohammadi, and G. Nikolakopoulos. 2022. "COMPRA: A Compact Reactive Autonomy Framework for Subterranean MAV Based Search-And-Rescue Operations." *Journal of Intelligent & Robotic Systems* 105: 49. <https://doi.org/10.1007/s10846-022-01665-6>.
- Paolo Valpolini. 2020. "SpearUAV Unveils Ninex – a Unique Encapsulated Drone System for Instant ISTAR Capabilities." *European Defence Review*. <https://www.edrmagazine.eu/spearuav-unveils-ninox-a-unique-encapsulated-drone-system-for-instant-istar-capabilities>.
- Petrís, P. D., H. Nguyen, M. Dharmadhikari, et al. 2022. "RMF-Owl: A Collision-Tolerant Flying Robot for Autonomous Subterranean Exploration." In *2022 International Conference on Unmanned Aircraft Systems (ICUAS)*, 536–543. IEEE.
- Petrlik, M., P. Petráek, V. Krátký, et al. 2025. "UAVs Beneath the Surface: Cooperative Autonomy for Subterranean Search and Rescue

in Darpa SubT.” In *IEEE Transactions on Field Robotics*, Vol. 2, 643–689. <https://doi.org/10.1109/TFR.2024.3492160>.

PowerVision. 2023. Poweregg Product Specifications. PowerVision Inc. <https://www.powervision.me/en/product/poweregg/specs>.

Rail, N. 2019. *Challenge Statement—Mining Ground Investigations*. Technical report. <https://www.networkrail.co.uk/wp-content/uploads/2019/06/Mining-Mining-Ground-Investigations.pdf>.

Riviere, V., A. Manecy, and S. Viollet. 2018. “Agile Robotic Fliers: A Morphing-Based Approach.” *Soft Robotics* 5, no. 5: 541–553. PMID: 29846133.

Rouček, T., M. Pecka, P. Čížek, et al. 2020. “Darpa Subterranean Challenge: Multi-Robotic Exploration of Underground Environments.” In, edited by J. Mazal, A. Fagiolini, P. Vasik, 274–290. Cham. Springer International Publishing.

Schleich, D., M. Beul, J. Quenzel, and S. Behnke. 2021. “Autonomous Flight in Unknown GNSS-Denied Environments for Disaster Examination.” In *2021 International Conference on Unmanned Aircraft Systems (ICUAS)*, 950–957. IEEE.

Tavasoli, S., X. Pan, and T. Yang. 2023. “Real-Time Autonomous Indoor Navigation and Vision-Based Damage Assessment of Reinforced Concrete Structures Using Low-Cost Nano Aerial Vehicles.” *Journal of Building Engineering* 68: 106193.

Tranzatto, M., T. Miki, M. Dharmadhikari, et al. 2022. “CERBERUS in the DARPA Subterranean Challenge.” *Science Robotics* 7, no. 66: eabp9742. <https://doi.org/10.1126/scirobotics.abp9742>.

Vadillo, I., J. Benavente, C. Neukum, et al. 2012. “Surface Geophysics and Borehole Inspection as an Aid to Characterizing Karst Voids and Vadose Ventilation Patterns (Nerja Research Site, S. Spain).” *Journal of Applied Geophysics* 82: 153–162.

Zhao, M., T. Anzai, F. Shi, X. Chen, K. Okada, and M. Inaba. 2018. “Design, Modeling, and Control of an Aerial Robot Dragon: A Dual-Rotor-Embedded Multilink Robot With the Ability of Multi-Degree-of-Freedom Aerial Transformation.” *IEEE Robotics and Automation Letters* 3, no. 2: 1176–1183.

Zhao, M., K. Kawasaki, X. Chen, S. Noda, K. Okada, and M. Inaba. 2017. “Whole-Body Aerial Manipulation by Transformable Multirotor With Two-dimensional Multilinks.” In *2017 IEEE International Conference on Robotics and Automation (ICRA)*, 5175–5182. IEEE.